Adv. Space Res. Vol. 7, No. 11, pp. (11)175–(11)180, 1987
Printed in Great Britain.

0273–1177/87 $0.00+.50

ON THE VARIABILITY OF ATMOSPHERE–BIOSPHERE EXCHANGE OF CO_2

I. Y. Fung*, C. J. Tucker** and K. C. Prentice*

*NASA/Goddard Space Flight Center, Institute for Space Studies, New York, NY 10025, U.S.A. and Lamont-Doherty Geological Observatory of Columbia University, Palisades, NY 10964, U.S.A.
**NASA/Goddard Space Flight Center, Greenbelt, MD 20771, U.S.A.

INTRODUCTION

The terrestrial biota plays a major role in the geographical and temporal variations of atmospheric CO_2 (Fig. 1a). The seasonal exchange of CO_2 between the atmosphere and the biosphere, via photosynthesis and soil release, is the primary cause of the annual oscillations found in the records of atmospheric CO_2 /1,2/. Analyses of the atmospheric CO_2 measurements show that the annual oscillations exhibit interannual variations and the amplitudes of the cycles have been increasing in time /2,3/. One of the possible contributing factors to the interannual and long-term variations is enhanced summer assimilation by the biosphere, although there is little field evidence to confirm this hypothesis.

Simulations of atmospheric CO_2 concentrations at a few observing stations have been used to estimate the magnitude of this exchange (e.g., /1,4,5,6/). Because of the differences in the atmospheric transport models, the biospheric exchange functions that provided best fit to the observations differed by at least a factor of two. Furthermore, because the exchange functions are based on simple assumptions, they cannot be used to evaluate the year-to-year changes in biospheric activity of the contributions of these changes to the interannual variations of atmospheric CO_2.

In this paper, we use satellite and field data to quantify the geographic distributions of the seasonal exchange of CO_2 between the atmosphere and the terrestrial biota. The exchange functions thus obtained will be validated by their ability to reproduce the observed annual cycles of atmospheric CO_2 in a 3D tracer transport model.

METHOD

In the following, we describe separately the method to obtain the monthly distributions of the uptake and release of the carbon from the biosphere. As the distributions will be used as inputs to a 3-D tracer transport model with horizontal resolution of 4° latitude x 5° longitude, the description will include the procedure to interpolate the fluxes to the appropriate grid.

Uptake of Carbon

During the process of photosynthesis, about 70 percent of the radiation in the visible spectrum incident on a leaf is absorbed by the chloroplast pigments in the leaf, and only less than 10 percent of the radiation in the near-infrared spectrum (0.7-1.1 μm) is absorbed. The remainder radiation in these spectral regions is reflected, transmitted or scattered. When the leaf senesces, there is a decrease in the absorbed fraction of incident visible radiation as well as in the reflected fraction of near-infrared radiation /7/. Hence, combinations of reflected radiances from the visible and near-infrared spectral regions are routinely used to estimate the green leaf biomass of plant canopies /8/. One commonly used combination is the 'normalized difference vegetation index' (NDVI), derived as a combination of C_1 and C_2, the radiances measured in the visible and in the near-infrared spectral regions respectively:

$$\text{NDVI} = \frac{C_2 - C_1}{C_1 + C_2} \tag{1}$$

In a few short-duration studies, the NDVI has been correlated with the green biomass in agricultural plots which are spatially homogeneous, and in the Senegalese Sahel region where vegetation is predominantly grassland (e.g. /9,10/).

Satellite remote sensing provides a potential means of monitoring and quantifying the temporal and spatial variations in the behavior of the terrestrial biota. The TIROS-N series of satellites of the

National Oceanic and Atmospheric Administration (NOAA) are well-suited to provide global data on a near-daily basis for the observation of vegetation dynamics. Channel 1 (0.55-0.68 μm) and Channel 2 (0.73-1.1 μm) radiances from the advanced very high resolution radiometer (AVHRR) sensor aboard the polar-orbiting satellites are collected daily at 4km-resolution for the entire surface of the globe. These data are referred to as Global Area Coverage (GAC) data. NDVI computed from the GAC data have been used to study continental land cover, global phyto-phenological phenomena, and grassland net primary production using multitemporal data for 1- to 4-year period /10/.

Weekly NDVI composites for the globe, as derived from radiances measured by the AVHRR on board NOAA-7 satellite, have been obtained for the period April 1982 to October 1984. The process of composting selects, for each location and time period, the maximum NDVI for the period, thereby minimizing the effects of sun angle, off-nadir viewing, atmospheric pathlength, aerosols and cloud, all of which only decrease the NDVI. Monthly composite NDVIs were formed from the weekly composites and the data were reaggregated to 4° latitude x 5° longitude resolution for the globe. Fig. 1b shows the latitudinal and temporal variations on the monthly NDVI composites, weighted by land areas in each latitude zone. Consistent with the general notions of the timing of the growing season, the NDVI in the northern hemisphere is high in spring/summer and is low in the autumn/winter. In the equatorial regions, the NDVI is high and remains relatively constant throughout the year.

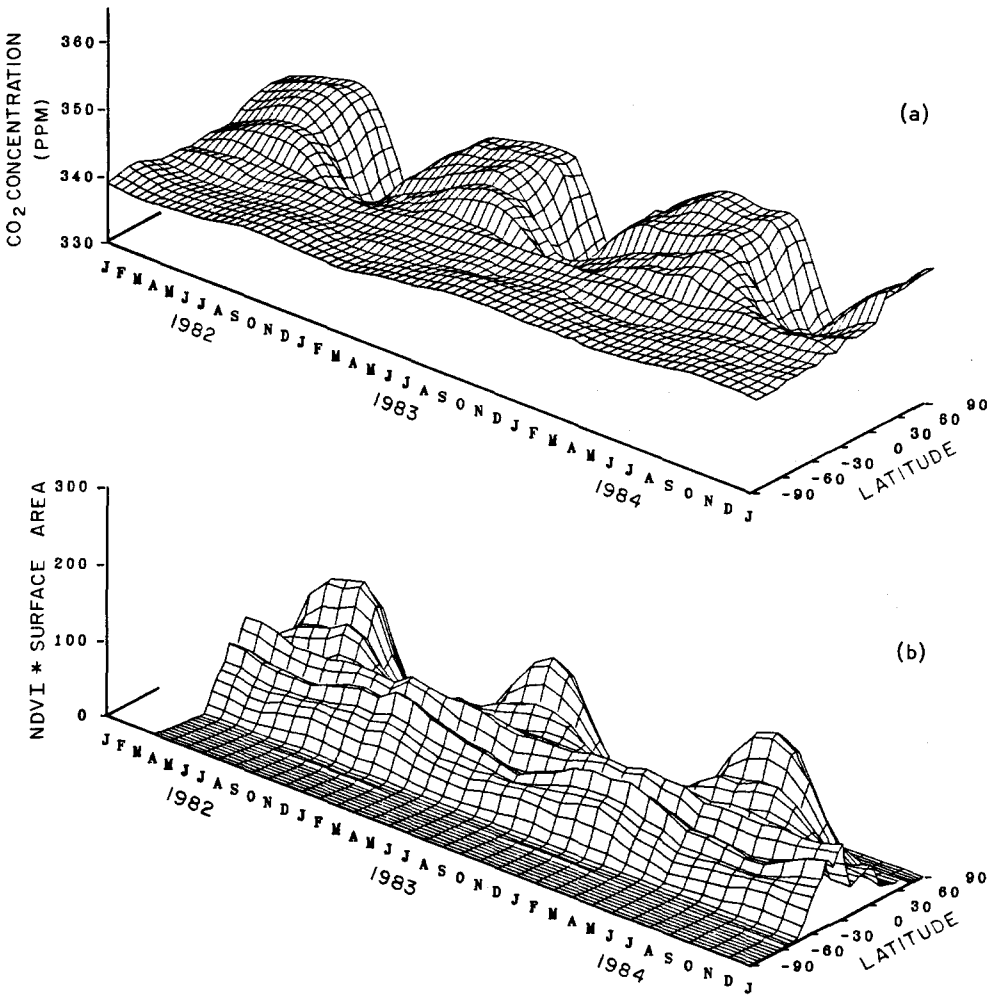

Fig. 1. Latitudinal and temporal variations of (a) atmospheric CO_2 and (b) the NDVI from 1982 to 1984. The atmospheric CO_2 data are obtained from the globally distributed monitoring network of NOAA/GMCC. The monthly NDVI composite data at 4°x5° resolution for the globe have been longitudinally weighted by land area in each 4° latitude zone.

A comparison of the NDVI with atmospheric CO_2 data is shown in Fig. 2. Monthly drawdown rate of atmospheric CO_2 has been calculated from the NOAA/GMCC data for 1982 - 1984, and is shown by the solid lines in Fig. 2. The zonally averaged NDVI is shown as the shaded regions. At mid-latitudes in the northern hemispheres where the annual cycles of atmospheric CO_2 is dominated by exchanges with the biota /2/, there is remarkable correspondence between the duration of high NDVI and the duration of CO_2 drawdown as well as between the timing of the maximum drawdown of CO_2 and the timing of the peak NDVI. This agreement suggests that the NDVI may be used as an indicator of the phasing of the photosynthetic uptake of CO_2 from the atmosphere.

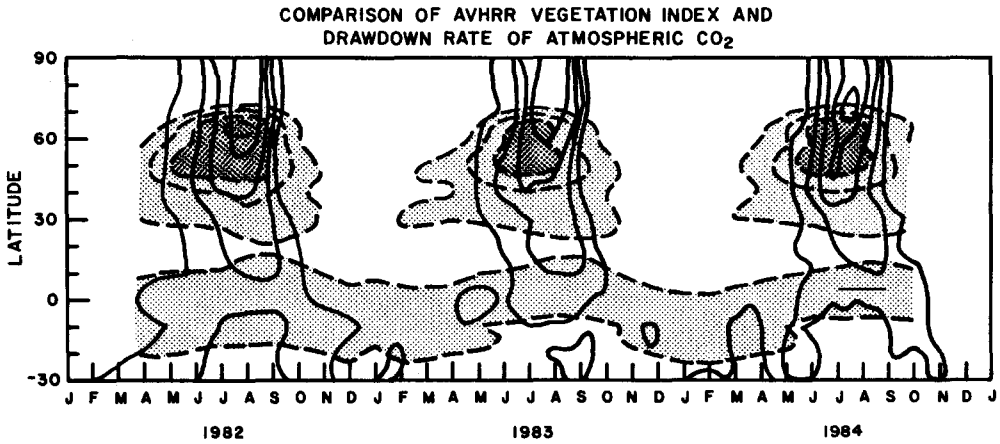

Fig. 2. Comparison of the drawdown rate of (solid lines) with the NDVI (shaded regions). CO_2 drawdown rate is contoured at 2 ppm/month. The NDVI has been zonally averaged over all surface areas in a latitude belt. The NDVI is contoured at 0.1.

While the previous discussion indicates that the photosynthetic uptake of carbon is a monotonic function of the NDVI, the exact functional dependence of the uptake on NDVI remains to be found. In two recent studies, Asrar *et al.* /11/ and Sellers /12/ have demonstrated a near-linear relationship between the NDVI and the intercepted fraction of photosynthetically active radiation, the driving energy for photosynthesis. Also, a linear relationship has been found by Goward *et al.* /13/ between the integral of the NDVI from April to November and the annual net primary productivity of vegetation types in North America. Tucker *et al.* /14/ have also demonstrated that there is an approximately linear relationship between the detrended atmospheric CO_2 concentrations and the NDVI. On the other hand, other authors (e.g. /11,15/) have shown that the green leaf area index (LAI) of agricultural crops is a curvilinear function of the NDVI. The NDVI levels off, or saturates, at high values of LAI, with different saturation points for different crop species.

In this study, we assumed that the monthly uptake of carbon by photosynthesis is dependent on the exponent of the monthly NDVI, at each location, and that the annual integral of the monthly uptake is equal to the annual net primary productivity (NPP). In this way, we translate the non-dimensional NDVI into a dimensional carbon flux. The NPP at each location is derived from the NPP based on Whittaker and Likens /16/ applied to the 1° x 1° global vegetation map of Matthews /17/ and reaggregated to 4° x 5° model resolution. We note that we have also investigated a linear relationship between carbon uptake and the NDVI. In this model, a linear relationship was not chosen, as it underestimates the summer drawdown and seasonal amplitude of atmospheric CO_2.

It should be recognized that the radiances measured by the satellite sensor are the combined effects of the radiative properties of the surface as well as of the intervening atmospheric pathlength. Hence, variations in the atmospheric pathlength an in atmospheric composition as well as variations of the surface properties could affect the value of the NDVI. In this study, we have used the NDVI at a location to define only the phasing of the photosynthetic uptake of carbon. The magnitude of the atmospheric effects on the NDVI can only be ascertained by a full radiative transfer calculation.

Release of carbon

The other component of the seasonal exchange of CO_2 between the atmosphere and the terrestrial surface is the release of CO_2 from the biota when the detrital pool of carbon decomposes, Because the detrital pool has little or no chlorophyll and because the soil is generally obscured from the satellite's view by the vegetation, satellite observations do not provide sufficient information about the decomposition of the detritus or the phasing of the return of carbon from the soil to the atmosphere.

It is well known that the rate of CO_2 evolution from the soils is controlled, to a large extent, by the local climate /18/. The Van't Hoff reaction-rate/temperature rule uses the coefficient Q_{10} to express the increase in reaction rate resulting from a 10°C increase in temperature. It is recognized, however, that Q_{10} can vary by a factor of two to three with temperature and may vary with vegetation and soil type (see e.g. /19/). Instead of choosing Q_{10} values for each vegetation type, we have attempted to derive the temperature dependence of soil respiration directly from published field data.

Published field data on CO_2 fluxes throughout the year from the soils and the accompanying environmental temperatures have been compiled and digitized. These long time series are from 20 sites around the globe and have been organized into four major biome groups. These biome groups are: three woody vegetation types (temperate-boreal needle-leaved forests, woodlands and shrublands, temperate-boreal broad-leaved forests and woodlands, and tropical/subtropical forests and woodlands), and grasslands.

Linear regression analysis of soil release of carbon against *in situ* surface air temperature has been attained for each of the biome groups. For a typical temperature range of 0°C-20°C, the regression equations yield a Q_{10} of 1.4-1.7 for the needle-leaved woody vegetation, and a Q_{10} of 1.6-2.6 for the broad-leaved woody vegetation. For a temperature range of 10°C-30°C, Q_{10} is 1.4-1.7 for tropical/subtropical woody vegetation, and is 1.5-1.9 for grasslands. These Q_{10} values thus obtained are within the range of Q_{10} values of 1.5-3.2 frequently cited in the literature. By using the regression equations, we have incorporated the variations of Q_{10} within a temperature range, and between broad biome groups.

To obtain the global distribution of the monthly release of carbon from the soils, we use the linear regression equations and a global distribution of monthly surface air temperature /20/ to define the timing of the CO_2 release. The magnitude of the release is obtained by assuming that the annual release of carbon is equal to the annual uptake, so that a steady state biosphere exists.

3D Tracer Model

To test the reality of the formulations of the biospheric exchange of CO_2, we used the monthly net exchange of CO_2 described above as source/sink functions in a 3D tracer transport model to simulate the variations of CO_2 in the atmosphere. The 3D tracer model uses winds from the General Circulation Model II (GCM) at the Goddard Institute for Space Studies (GISS) to advect CO_2 as an inert trace constituent. The tracer model has been described /6,21/. The version of the model used in those studies have horizontal resolutions of 8° latitude x 10° longitude. The version of the model used here employs winds and sub-grid scale convective fluxes from the fine-grid (4° latitude x 5° longitude) version of the GCM. All physical processes in the GCM are identical to those described in Hansen *et al.* /22/. The fine-grid version of the GCM has improved simulation of the strength and position of the Hadley circulation, synoptic scale features, as well as the higher moments statistics of the general circulation.

RESULTS AND DISCUSSION

The approach described obtained, using available satellite and field data, global distributions of the seasonal exchange of CO_2 between the atmosphere and the terrestrial biosphere. The atmospheric CO_2 distribution resulting from this exchange has been simulated using the 3-D tracer model. In the northern hemisphere, the modeled annual cycles of CO_2 show reasonable agreement with those observed at remote monitoring sites. A comparison of the simulated and observed oscillations at three locations is shown in Fig. 3.

At Mauna Loa, Hawaii, the modeled and observed CO_2 oscillations have peak-peak amplitudes of ~6ppm, with the maximum in May and the minimum in October. At Pt. Barrow, Alaska, the modeled CO_2 concentrations, like those observed, peak in May and decrease rapidly by ~16 ppm to a minimum in September/October. From October to November, the modeled atmospheric CO_2 concentration rapidly increases due to soil respiration. In this study, we have assumed that soil respiration was turned off when air temperature fell below -10°C, resulting a slower winter increase in atmospheric CO_2 than is observed. The rise in CO_2 from November to February is caused primarily by CO_2 from the southern latitudes transported northwards or across the pole. CO_2 resumes its rapid increase after February with the spring thaw in high latitudes. This lack of agreement between the observed and simulated CO_2 concentrations in winter may be caused by the neglect of litter amount and moisture availability on the rate of heterotrophic respiration. At Ocean Weather Ship Papa, the CO_2 drawdown rate is well simulated. CO_2 concentration peaks in May, and decreases rapidly by ~12 ppm in 3-4 months to a minimum in September. However, like Pt. Barrow, the simulated shape of the winter increase in CO_2 differs from that observed, probably due to the treatment of soil respiration in the model.

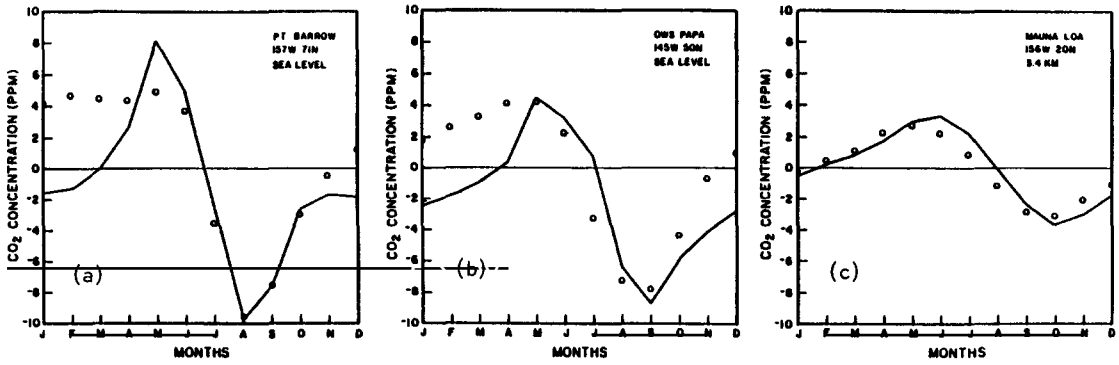

Fig. 3. Comparison of simulated (solid lines) and observed (circles) annual cycles of atmospheric CO_2 at (a) Pt. Barrow, Alaska (175W, 71N), (b) Ocean Weather Ship Papa (145W, 50N), and (c) Mauna Loa, Hawaii (156W, 20N).

Similar agreement is found between the simulated and observed cycles of atmospheric CO_2 at all the remote monitoring sites in the northern hemisphere. These results demonstrate that the rate of photosynthetic drawdown of CO_2 by the biosphere can be derived from the NDVI. They also suggest that the empirical relationships between soil respiration and surface air temperatures may be a reasonable first attempt to obtain the seasonality of CO_2 evolution from the soils. The effects of moisture, litter amount and other abiotic factors on heterotrophic respiration must be included in future investigations.

The availability of the satellite-derived NDVI at high temporal resolution for the entire terrestrial surface allows, for the first time, the monitoring and inventory of terrestrial productivity and its variations on a global scale. Using the NOAA/AVHRR NDVI from 1982-1984 (Fig. 2), we have computed the mean monthly NDVI for each latitude zone, and the departures of the monthly NDVI from the three-year means for each month. The NDVI was higher from June-August 1982 in the latitude zones of 40°N-70°N. The drawdown rate of atmospheric CO_2 was likewise computed from the NOAA/GMCC atmospheric CO_2 observations and showed a larger drawdown rate during the same period for the same region. The agreement in both the timing and location of these anomalies suggest that the terrestrial biosphere of the Northern Hemisphere was more active photosynthetically in the summer of 1982 than in 1983 and 1984. This increase in the uptake of CO_2 in the atmosphere, if acting alone, would have increased the amplitudes of oscillations of atmospheric CO_2 by 50%. As the atmospheric CO_2 measurements show less than 10% change during this period, we argue that the climatic perturbations that favored enhanced productivity in the Northern Hemisphere summer also favored enhanced decomposition and release of the CO_2 to the atmosphere.

REFERENCES

1. L. Machta, Mauna Loa and global trends in air quality, *Bull. Am. Meteorol. Soc.*, *53*, 402-420 (1972)

2. C.D. Keeling, The global carbon cycle: What we know and could know from atmospheric, biospheric and oceanic observations, in: *Proceedings: Carbon Dioxide Research Conference: Carbon Dioxide, Science and Consensus, Berkeley Springs, West Virginia.* U.S. Department of Energy CONF-820970, U.S. Dept. of Energy, 1983.

3. G. Pearman and P. Hyson, The annual variation of atmospheric CO_2 concentration observed in the northern hemisphere, *J. Geophys. Res.*, *86*, 9839-9843 (1981)

4. C. Junge, and G. Czeplak, Some aspects of the seasonal variation of carbon dioxide and ozone, *Tellus*, *20*, 422-434 (1968)

5. G. Pearman and P. Hyson, Activities of the global biosphere as reflected in atmospheric CO_2 records, *J. Geophys. Res.*, *85*, 4457-4467 (1980)

6. I. Fung, K. Prentice, E. Matthews, J. Lerner and G. Russell, Three-dimensional tracer model study of atmospheric CO_2: Response to seasonal exchanges with the terrestrial biosphere, *J. Geophys. Res.*, *88*, 1281-1294 (1983)

7. C.J. Tucker and M. Garrett, Leaf optical system modeled as a stochastic process, *Appl. Opt.*, *16*, 635-642 (1977)

8. C.J. Tucker, A critical review of remote sensing and other methods for nondestructive estimation of standing crop biomass, *Grass Forage Sci.*, *35*, 177-182 (1980)

9. C.J. Tucker, B.N. Holben, J.H. Elgin, and J.E. McMurtrey, Remote sensing of total dry matter accumulation of winter wheat, *Remote Sens. Environ.*, *11*, 171-189 (1981)

10. C.J. Tucker, C. Vanpraet, E. Boerwinkel and A. Gaston, Satellite remote sensing of total dry matter production in the Senegalese Sahel, *Remote Sens. Environ.*, *13*, 461-474 (1983)

11. G. Asrar, M. Fuchs, E.T. Kanemasu, and J.L. Hatfield, Estimating absorbed photosynthetic radiation and leaf area index from spectral reflectance in wheat, *Agron. J.*, *76*, 300-306 (1984)

12. P.J. Sellers, Canopy reflectance, photosynthesis and transpiration, *Int. J. Remote Sens.*, *6*, 1335-1372 (1985)

13. S.N. Goward, C.J. Tucker and D.G. Dye, North American vegetation patterns observed with the NOAA-7 Advanced Very High Resolution Radiometer, *Vegetatio*, *64*, 3-14 (1986)

14. C.J. Tucker, I.Y. Fung, C.D. Keeling and R.H. Gammon, Relationship between atmospheric CO_2 variations and a satellite-derived vegetation index, *Nature*, *319*, 195-199 (1986)

15. P.J. Curran, Multispectral remote sensing for the estimation of greenleaf area index, *Philos. Trans. R. Soc. Lond, Ser. A*, *309*, 257-270 (1983)

16. R.H. Whittaker and G.E. Likens, The biosphere and man, in: H. Lieth and R. H. Whittaker, eds., *Primary Productivity of the Biosphere*, Ecological Studies 14, Springer-Verlag, New York, pp. 305-328, 1975.

17. E. Matthews, Global vegetation and land use: new high-resolution data bases for climate studies, *J. Clim. Appl. Meteorol.*, *22*, 474-487 (1983)

18. J.S. Singh and S.R. Gupta, Plant decomposition and soil respiration in terrestrial ecosystems, *Bot. Rev.*, *43*, 449-528 (1977)

19. W. Larcher, *Physiological Plant Ecology*, 303 pp., Springer-Verlag, New York, 1980.

20. C. Schutz and W.L. Gates, Global climatic data for surface, 800 mb, 400 mb; January, *Rep. R-95-ARPA*, Rand Corp., Santa Monica, Calif. (1971)

21. I. Fung, Analysis of the seasonal and geographical patterns of atmospheric CO_2 distributions with a 3-D tracer model, in: J.R. Trabalka and D.E. Reichle, eds., *The Changing Carbon Cycle: A Global Analysis*, 459-473, Springer-Verlag, New York, 1986.

22. J. Hansen, G. Russell, D. Rind, P. Stone, A. Lacis, S. Lebedeff, R. Ruedy, and L. Travis, Efficient three-dimensional global models for climate studies: Models I and II, *Mon. Weather Rev.*, *111*, 609-662 (1983)